AFRL-VS-HA-TR-98-0079

MODIFICATIONS AND IMPROVEMENTS TO THE PRISM AND PIM IONOSPHERIC MODELS

Robert E. Daniell, Jr.
Lincoln D. Brown
Raymond P. Barnes

Computational Physics, Inc.
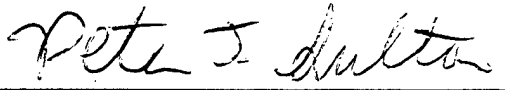240 Bear Hill Road, Suite 202A
Waltham, MA 02451

15 June 1998

Scientific Report No. 1

19990126 033

AIR FORCE RESEARCH LABORATORY
Space Vehicles Directorate
29 Randolph Road
AIR FORCE MATERIEL COMMAND
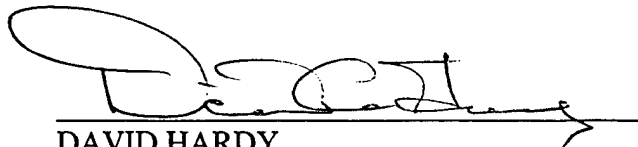**HANSCOM AFB, MA 01731-3010**

DTIC QUALITY INSPECTED 3

This technical report has been reviewed and is approved for publication.

PETER J. SULTAN
Contract Manager

ROBERT MORRIS
Branch Chief

DAVID HARDY
Division Director

REPORT DOCUMENTATION PAGE

Public reporting burden for this collection of information is estimated to average 1 hour per response, including the time for reviewing instructions, searching existing data sources, gathering and maintaining the data needed, and completing and reviewing the collection of information. Send comments regarding this burden estimate or any other aspect of this collection of information, including suggestions for reducing this burden, to Washington Headquarters Services, Directorate for Information Operations and Reports, 1215 Jefferson Davis Highway, Suite 1204, Arlington, VA 22202-4302, and to the Office of Management and Budget, Paperwork Reduction Project (0704-0188), Washington, DC 20503.

1. AGENCY USE ONLY (Leave blank)	2. REPORT DATE 15 June 1998	3. REPORT TYPE AND DATES COVERED Scientific No. 1 (25 Jul 95 - 10 Aug 96)

4. TITLE AND SUBTITLE
Modifications and Improvements to the PRISM and PIM Ionospheric Models

5. FUNDING NUMBERS

6. AUTHOR(S)
Robert E. Daniell, Jr., Lincoln D. Brown, and Raymond P. Barnes*

Contract F19628-95-C-0079

7. PERFORMING ORGANIZATION NAME(S) AND ADDRESS(ES)
Computational Physics, Inc.
240 Bear Hill Road, Suite 202A
Waltham, MA 02451

8. PERFORMING ORGANIZATION REPORT NUMBER

9. SPONSORING / MONITORING AGENCY NAME(S) AND ADDRESS(ES)
Air Force Research Laboratory
29 Randolph Street
Hanscom AFB, MA 01731-3010
Contract Manager: Peter Sultan/VSBP

10. SPONSORING / MONITORING AGENCY REPORT NUMBER
AFRL-VS-HA-TR-98-0079

11. SUPPLEMENTARY NOTES
*Computational Physics, Inc., 2750 Prosperity Avenue, Suite 600, Fairfax, VA 22031

12A. DISTRIBUTION / AVAILABILITY STATEMENT

APPROVED FOR PUBLIC RELEASE;
DISTRIBUTION UNLIMITED

12b. DISTRIBUTION CODE

13. ABSTRACT (Maximum 200 words)

This report describes the preliminary design of PRISM Version 2, a parameterized, real-time ionospheric specification model. PRISM was developed for use at the 55th Space Weather Squadron (55SWXS) at Falcon Air Force Base. PRISM consists of the theoretical climatology model, PIM (Parameterized Ionospheric Model), and an algorithm for updating PIM electron density profiles using ground based and spaced data. The new versions of PIM and PRISM will be based on a single, global, physics-based ionospheric model that incorporates the plasmasphere. They will be parameterized in terms of month (rather than season), and with additional climatological parameters augmenting the solar activity and geomagnetic activity parameters of the old version. PRISM 2 will also have an improved data assimilation algorithm. This report also describes modifications to VOACAP to allow it to read and use the PIM or PRISM ionosphere instead of its own internal ionosphere and other updates to the operational version of PRISM.

14. SUBJECT TERMS
ionosphere, space environment, data assimilation, space weather, ionospheric specification

15. NUMBER OF PAGES
44

16. PRICE CODE

17. SECURITY CLASSIFICATION OF REPORT Unclassified	18. SECURITY CLASSIFICATION OF THIS PAGE Unclassified	19. SECURITY CLASSIFICATION OF ABSTRACT Unclassified	20. LIMITATION OF ABSTRACT SAR

Table of Contents

This page is intentionally blank.

Executive Summary

During the first year of this contract, Computational Physics, Inc. (CPI) began the process of developing a new version of the Parameterized Real-time Ionospheric Specification Model (PRISM) to be known as PRISM 2. The current version of PRISM was developed by CPI under previous contracts and is operational at the 55th Space Weather Squadron (55 SWXS) at Falcon AFB. It is a parameterization of a combination of physics-based regional ionospheric models developed at several institutions, and it includes the capability of ingesting near-real-time ionospheric data and updating its theoretical climatology to provide an accurate specification of the current state of the ionosphere. It can, of course, also be used for post-event analysis. The Parameterized Ionospheric Model (PIM) is essentially PRISM without the capability of using ionospheric data to update its theoretical climatology.

The new version, PRISM 2, will be a parameterization of a single, truly global, physics based ionospheric model, the Global Theoretical Ionospheric Model (GTIM) developed under the auspices of the Battlespace Environment Division of the Space Vehicles Directorate of the Air Force Research Laboratory (AFRL). Because GTIM is being upgraded to include the light ions (H^+ and He^+), and thus the plasmasphere, PRISM 2 will also include the plasmasphere. As a result of the continuing computer revolution, which permits many more GTIM runs to be used in the parameterization, PRISM 2 will also incorporate additional input parameters: besides solar activity, geomagnetic activity, and high latitude convection parameters, PRISM 2 will also use longitude dependent wind and equatorial drift parameters. It will also use monthly (rather than seasonal) coefficients with the capability of interpolating on Julian date. Finally, the data assimilation algorithm in PRISM will be upgraded to make better use of TEC data.

In addition to describing the initial design of PRISM 2, this report also describes the continuing updates of the operational version of PRISM, and the modification of IONCAP/VOACAP to read PRISM output.

1. INTRODUCTION

The primary objective of this contract is the extension of the Parameterized Real-time Ionospheric Specification Model (PRISM) to include the plasmasphere. The present version of PRISM extends only to 1600 km and is probably valid only to about 1200 km. The extension will be accomplished by adding a parameterized model of the plasmasphere to PRISM. The new version of PRISM will be called PRISM 2.0 and will incorporate a number of other improvements. Secondary objectives include (1) continued support for PRISM 1.6, which is the operational version at the 50th Weather Squadron at Falcon AFB, (2) the development of PRISM applications such as three-dimensional ray tracing software, and (3) the development of visualization software for use with PRISM output.

The emphasis of the first year of this contract was on preliminary development tasks for PRISM 2.0. Additionally, we have modified VOACAP (an updated version of IONCAP) so that it can read PRISM output files and use the PRISM ionosphere in place of its internal ionosphere for calculating HF propagation predictions. Modifications to the current version of PRISM to correct problems that have been uncovered by various PRISM users are described in Appendix A.

The content of this report reflects the state of the effort as of August 1996. Many things have changed since then, and the reader is urged to consult later reports in this series for more current descriptions of PRISM development.

2. THE HIGH ALTITUDE EXTENSION TO PRISM AND PIM

The Parameterized Real-time Ionospheric Specification Model (PRISM) has been described by *Daniell et al.* [1990] and *Anderson* [1993]. The climatological model on which PRISM is based, known as PIM, has been described by *Daniell et al.* [1995]. The validation of an early version of PRISM was described by *Daniell et al.* [1993]. Since those reports, a number of modifications have been made, and the model has undergone transition to operational use at the 55th Weather Squadron (55 SWXS, formerly the 50th Weather Squadron, formerly the Space Forecast Center) at Falcon Air Force Base. Ionospheric products produced by 55 SWXS using PRISM are made available to DoD customers and, through NOAA's Space Environment Center, to civilian customers as well.

We are in the process of developing a substantially new version, PRISM 2.0, that incorporates a number of improvements including (1) improved theoretical climatology, (2) a plasmasphere model, and (3) an improved fully analytic functional representation. These and other modifications are described in this section.

2.1 Theoretical Climatology and the Plasmasphere Model

The first version of PRISM was based on a collection of regional ionospheric models which had to be merged at the region boundaries. The new version will be based on a single,

global ionospheric model: the Global Theoretical Ionospheric Model (GTIM) developed by the Space Vehicles Directorate of the Air Force Research Laboratory. The model was derived from LOWLAT, originally developed by *Anderson* [1973]. The model is being expanded to include high-latitude convection and auroral ionization, E-region chemistry, and the light ions of the plasmasphere. The high-latitude extension has been described by *Decker et al.* [1994]. The plasmasphere is being included by separately solving the transport equations for O^+, H^+, and He^+ (in that order) at each time step. It appears that by using a short enough time step, it is not necessary to iterate the solution.

For the climatological runs, we plan to run the model for a sufficient number of days to fill the flux tubes up to the plasmapause. However, we also plan to save the plasma distribution for the outer field lines once each day, and use this to produce a model of the refilling of the flux tubes after a magnetic storm. This will be used to produce a more realistic plasmasphere specification even in the absence of real-time data.

Since GTIM solves only the coupled ion continuity equations, it requires a thermospheric density and composition model, a thermospheric wind model, electron and ion temperature models, a high-latitude horizontal convection model, and a low-latitude vertical convection model, and a high-latitude electron and ion precipitation model. We have chosen MSIS-90 as the thermospheric model, HWM-90 as the thermospheric wind model. The electron and ion temperature model is based on *Brace and Theis* [1981] with our own method for producing temperature profiles. (See Appendix B.) The high-latitude horizontal convection model is that of *Rich and Maynard* [1989], which is an analytic form of the empirical model of *Heppner and Maynard* [1987]. The high-latitude auroral precipitation is modeled using the electron precipitation model of *Hardy et al.* [1987] and the ion precipitation model of *Hardy et al.* [1991]. The low-latitude vertical convection model is based on *Fejer et al.* [1995] with modifications to the nighttime drift to ensure diurnal reproducibility.

2.2 Functional Representation of the Climatology

PIM and PRISM 2.0 will incorporate a fully analytic (albeit quite complicated and very non-linear) functional representation of the ionospheric climatology. The coordinate system used in the functional representation is a geomagnetic system with coordinates (z, λ, φ) where φ is geomagnetic longitude, λ is geomagnetic latitude, and z is altitude. The electron density is calculated from the following equations:

$$n_e(z, \lambda, \varphi, \tau) = \sum_{i=1}^{S} n_i(z, \lambda, \varphi, \tau) \tag{1}$$

where τ is Universal Time (expressed as an angle: $\tau = \pi \times UT / 12$). PRISM 2.0 will have five ion species, O_2^+, NO^+, O^+, He^+, and H^+. Each ion species will be represented by functions of the form

2

$$\ln n_i(z,\lambda,\varphi,\tau) = \ln N_i(\lambda,\varphi,\tau) + 1 - x - e^{-x} + \sum_{j=0}^{J} \alpha_j^{(i)}(\lambda,\varphi,\tau) P_j^{(i)}(x), \quad x = \frac{z - h_i(\lambda,\varphi,\tau)}{H_i(\lambda,\varphi,\tau)} \quad (2)$$

$$\ln N_i(\lambda,\varphi,\tau) = \sum_{k=0}^{K} \sum_{l=-L}^{L} \sum_{m=-M}^{M} a_{klm}^{(i)} p_k(\lambda) e^{il\varphi} e^{im\tau} \quad (3)$$

$$h_i(\lambda,\varphi,\tau) = \sum_{k=0}^{K} \sum_{l=-L}^{L} \sum_{m=-M}^{M} b_{klm}^{(i)} p_k(\lambda) e^{il\varphi} e^{im\tau} \quad (4)$$

$$H_i(\lambda,\varphi,\tau) = \sum_{k=0}^{K} \sum_{l=-L}^{L} \sum_{m=-M}^{M} c_{klm}^{(i)} p_k(\lambda) e^{il\varphi} e^{im\tau} \quad (5)$$

$$\alpha_j^{(i)}(\lambda,\varphi,\tau) = \sum_{k=0}^{K} \sum_{l=-L}^{L} \sum_{m=-M}^{M} \beta_{jklm}^{(i)} p_k(\lambda) e^{il\varphi} e^{im\tau} \quad (6)$$

where the functions $P_j(x)$ and $p_k(\lambda)$ are orthogonal polynomials. Note that the requirement that all quantities be real imposes conditions on the coefficients:

$$a_{klm}^{(i)} = \left[a_{k,-l,-m}^{(i)} \right]^* \quad (7)$$

and similarly for the other coefficients.

2.3 Climatological Parameters

Earlier versions of PIM and PRISM were parameterized in terms of (1) season, (2) solar activity, and (3) magnetic activity. In order to provide a better representation of the annual variation, Version 2 of PIM and PRISM incorporates monthly coefficient sets with interpolation to provide a coefficient set for the nominal date of the run. In order to provide a more accurate representation of the solar activity variation of the run, PIM and PRISM 2 are parameterized in terms of Q_{EUV} [*Strickland et al.*, 1995], a measure of the integrated solar EUV flux shortward of 45 nm with units of erg cm^{-2} s^{-1}. This is much more representative of the ionizing power of the sun than either $F_{10.7}$ (the radio flux at 2800 MHz) or the sunspot number. Q_{EUV} will be routinely produced by the SSUSI (Special Sensor Ultraviolet Spectrographic Imager) on DMSP satellites near the end of this decade, and (probably) on the follow-on NPOES satellites early in the next century. In the meantime, we will assume the following linear relationship between Q_{EUV} and $F_{10.7}$:

$$F_{10.7} = 70 + 54(Q_{EUV} - 1) \quad (8a)$$

$$Q_{EUV} = 1 + \frac{F_{10.7} - 70}{54} \quad (8b)$$

3

As described in Appendix C, we will probably convert the Q_{EUV} value from SSUSI to another value based on the flux shortward of 100 nm (instead of 45 nm).

Two new climatological parameters have been added to PRISM: $\overline{W}_m^{(h)}(\varphi)$ and $\overline{D}_{eq}^{(j)}(\varphi)$. The first is a meridional wind parameter while the second is a low latitude vertical drift parameter. The bars are to remind us that they are time-averaged indices. Both are assumed to be functions of longitude. The wind parameter is defined separately for the northern and southern hemisphere and represents a scaling of the HWM90 wind model, the precise form of which is to be determined. $\overline{D}_{eq}^{(0)}(\varphi)$ scales the overall diurnal variation of the vertical drift, while $\overline{D}_{eq}^{(1)}(\varphi)$ scales the magnitude of the pre-reversal enhancement. As mentioned above, the nominal diurnal drift pattern will be derived from *Fejer et al.* [1995].

2.4 The Data Assimilation Algorithm

PRISM's data assimilation algorithm was described by *Daniell et al.* [1993]. It allows the theoretical climatology to be updated using actual data. In Version 1.4, we introduced a change in the algorithm allowing PRISM to ingest and make use of all data in a four hour window centered on the nominal UT of the run. The use of data from the preceding two hours increases the amount of data available, especially when data is late arriving at 50 WS. The use of data from the following two hours was introduced primarily to benefit post event analysis, i.e., when the model is being run after the fact. The data are used in the form of differences between each datum and the corresponding model prediction. For example, if an ionosonde reports f_oF_2 measurements every one-half hour, it will provide 9 measurements in a four-hour window. The f_oF_2 values are converted to Δf_oF_2 values where

$$\Delta f_oF_2 = f_oF_2^{(measured)} - f_oF_2^{(model)}$$

The current data assimilation algorithm effectively averages over all difference values in the four-hour window. Thus, although the algorithm was originally conceived to produce a data prediction error of zero, it no longer does so. Instead, it predicts the "mean correction" at each site with zero error.

Because of the addition of the plasmasphere model, additional data types will be added to the input, and some previously available data will be used differently. In addition to the K_p index, PRISM will require an eight day history of D_{st} (or its equivalent) to track the recovery after a magnetic storm. The plasmapause is assumed to coincide with the equatorward boundary of the high latitude convection. While PRISM currently has its own algorithm for identifying this boundary from drift meter data from the SSIES instrument on DMSP, we expect that this will eventually be done externally by a separately developed algorithm. The plasma content of flux tubes near the plasmapause is determined by the time that the flux tubes have been equatorward of the plasmapause. In situ measurements of H^+ density by the RPA component of the SSIES instrument will also be used to adjust the H^+ densities in the model. PRISM 2 will also be capable of ingesting other kinds of data relevant to the plasmasphere: TEC

measurements from dual frequency GPS receivers on orbiting satellites (e.g., DMSP) are one kind of data that may become available in the future and which are of direct relevance to the plasmasphere.

During the next fiscal year, we hope to upgrade the adjustment algorithm to allow the direct use of slant TEC. (Presently, PRISM requires slant TEC to be converted to vertical equivalent TEC external to PRISM.) This will require a generalization of the current adjustment algorithm.

3. MODIFYING VOACAP TO USE PRISM

Since many of the important customers for ionospheric information from the 55th Space Weather Squadron are interested in HF propagation parameters, and since 55th uses IONCAP to generate the HF parameters for its customers, and since PRISM is now the operational ionospheric model at 55th, we undertook to make IONCAP work with PRISM output. However, rather than work with IONCAP, we chose to work with VOACAP, an updated and corrected version of IONCAP.

The purpose of VOACAP is the calculation of parameters that influence frequency management for a specified "circuit" — that is, HF communication between two specified stations. VOACAP calculates its HF parameters by performing a crude ray trace through an ionosphere characterized by the electron density profile (EDP) at the midpoint of the circuit. From this EDP, VOACAP calculates a model ionogram from which it builds a reflectrix table that is used to find the ray sets that describe the propagation for the user selected operating frequency.

We have made no changes to the basic analysis performed by VOACAP, but we have modified VOACAP to read output from PIM or PRISM and substitute the PIM or PRISM EDP for VOACAP's internally generated EDP.

Examples of the VOACAP output using its internal ionosphere and PRISM are shown on the following pages

First, an example output file from VOACAP using its internal (CCIR based) ionosphere:

```
IONOSPHERIC COMMUNICATIONS ANALYSIS AND PREDICTION PROGRAM
            VOACAP   VERSION 96.0213




          1         2         3         4         5         6         7
12345678901234567890123456789012345678901234567890123456789012345

COMMENT    Any VOACAP default cards may be placed in the file: VOACAP.DEF
COEFFS     CCIR
TIME           1   24    1    1
MONTH      1998  617    0
SYSTEM         1. 145. 0.01   90.73.00 3.00 0.1
SUNSPOT    071.
METHOD         7    0
ANTENNA        1    1    2   30      .000[:[default]const17.voa]    .0     500.0000
ANTENNA        2    2    2   30      .000[:[default]swwhip.voa ]    .0       .0000
FREQUENCY  15.0 20.0 0.
LABEL      Bauru                Beverly Hills
CIRCUIT    22.32S  049.07W      34.07N   118.42W
EXECUTE
LABEL      Beverly Hills    Bauru
CIRCUIT    34.07N   118.42W     22.32S   049.07W
EXECUTE
QUIT
1     ccir Coefficients        ~METHOD  7    VOACAP 96.0213    PAGE    1

  Jun   17, 1998            SSN =  71.           Minimum Angle= 0.010 degrees
  Bauru                 Beverly Hills        AZIMUTHS        N. MI.        KM
  22.32 S   49.07 W - 34.07 N  118.42 W    309.07  119.88   5205.4    9639.6


                    ELAYER/F2LAYER                        F1LAYER(E)/ESLAYER

  GMT    LMT    FOT    MUF    HPF ANGLE VIRTL   TRUE FVERT     FOT    MUF    HPF ANGLE VIRTL   TRUE FVERT

  1.0   21.7    2.0    2.3    2.6   0.4  125.   104.   0.4     2.0    2.3    2.6   0.4  125.   104.   0.4
               15.1   19.9   27.8   7.9  452.   309.   6.5     5.0    8.2   15.1   2.1  110.   110.   1.5
  2.0   22.7    1.8    2.0    2.3   0.4  125.   104.   0.4     1.8    2.0    2.3   0.4  125.   104.   0.4
               15.1   20.4   27.1   7.3  432.   293.   6.5     4.6    7.5   13.5   2.1  110.   110.   1.4
  3.0   23.7    1.7    2.0    2.2   0.4  125.   104.   0.4     1.7    2.0    2.2   0.4  125.   104.   0.4
               15.1   20.4   27.1   6.6  411.   276.   6.2     4.5    7.3   12.3   2.1  110.   110.   1.4
  4.0    0.7    1.8    2.0    2.3   0.4  125.   104.   0.4     1.8    2.0    2.3   0.4  125.   104.   0.4
               14.7   19.8   26.4   6.1  395.   262.   5.9     4.5    7.3   11.3   2.1  110.   110.   1.4
  5.0    1.7    1.9    2.2    2.5   0.4  125.   104.   0.4     1.9    2.2    2.5   0.4  125.   104.   0.4
               14.0   18.9   25.2   5.8  384.   258.   5.5     4.4    7.1   10.7   2.1  110.   110.   1.3
  6.0    2.7    2.2    2.5    2.8   0.4  125.   104.   0.4     2.2    2.5    2.8   0.4  125.   104.   0.4
               12.6   17.7   24.4   5.6  380.   259.   5.2     4.2    6.8   10.4   2.1  110.   110.   1.3
  7.0    3.7    2.6    3.0    3.4   0.4  125.   104.   0.5     2.6    3.0    3.4   0.4  125.   104.   0.5
               11.3   16.0   22.0   5.6  378.   261.   4.7     4.1    6.7   10.7   2.1  110.   110.   1.2
  8.0    4.7    3.4    3.9    4.4   0.4  125.   104.   0.7     3.4    3.9    4.4   0.4  125.   104.   0.7
                9.9   14.0   19.3   5.6  379.   262.   4.1     4.4    7.0   11.6   2.1  110.   110.   1.3
  9.0    5.7    4.6    5.3    6.0   0.4  125.   104.   0.9     4.6    5.3    6.0   0.4  125.   104.   0.9
                9.1   12.8   17.7   5.7  383.   260.   3.8     5.1    8.3   19.5   2.1  110.   110.   1.5
 10.0    6.7    6.5    7.4    8.4   0.4  125.   104.   1.3     6.5    7.4    8.4   0.4  125.   104.   1.3
               11.9   13.9   16.3   6.1  396.   260.   4.1     5.7    9.3   20.1   2.1  110.   110.   1.7
 11.0    7.7    5.0    5.7    6.5   0.4  125.   104.   1.0     5.0    5.7    6.5   0.4  125.   104.   1.0
               10.1   16.0   23.0   7.0  423.   289.   5.0     6.4   10.5   21.4   2.1  110.   110.   2.0
 12.0    8.7    7.0    8.0    9.1   0.4  125.   104.   1.4     7.0    8.0    9.1   0.4  125.   104.   1.4
               13.9   16.6   18.4   6.9  419.   276.   5.1     6.2   10.2   21.7   2.1  110.   110.   1.9
 13.0    9.7    9.1   10.5   11.8   0.4  125.   104.   1.9     9.1   10.5   11.8   0.4  125.   104.   1.9
               16.0   19.1   21.1   6.9  421.   270.   5.8     6.6   10.8   22.9   2.1  110.   110.   2.0
 14.0   10.7   11.2   12.9   14.5   0.4  125.   104.   2.3    11.2   12.9   14.5   0.4  125.   104.   2.3
               18.4   21.9   24.3   7.2  428.   268.   6.7     7.4   12.3   24.7   2.1  110.   110.   2.3
 15.0   11.7   13.2   15.2   17.1   0.4  125.   104.   2.7    14.6   16.7   18.9   3.1  301.   186.   4.0
               19.1   22.8   25.3   8.0  454.   271.   7.1     8.6   14.3   26.7   2.1  110.   110.   2.7
 16.0   12.7   15.1   17.3   19.5   0.4  125.   104.   3.1    15.9   18.3   20.6   2.9  295.   178.   4.3
               18.7   22.0   28.2   8.8  482.   277.   7.1     9.8   16.3   28.6   2.1  110.   110.   3.1
 17.0   13.7   16.6   19.1   21.5   0.4  125.   104.   3.4    16.9   19.4   21.9   2.7  289.   170.   4.5
               18.7   22.0   28.2   9.4  501.   278.   7.2    10.6   17.7   30.7   2.1  110.   110.   3.3
 18.0   14.7   15.1   17.3   19.5   0.4  125.   104.   3.1    15.2   17.4   19.7   3.3  307.   182.   4.2
               19.5   23.8   30.0   2.6  612.   334.   7.5    10.8   18.0   32.8   2.1  110.   110.   3.4
 19.0   15.7   13.0   14.9   16.8   0.4  125.   104.   2.7    13.0   14.9   16.8   0.4  125.   104.   2.7
```

6

		17.4	21.2	26.8	10.7	546.	331.	7.6	10.8	18.0	31.5	2.1	110.	110.	3.4
20.0	16.7	10.6	12.1	13.7	0.4	125.	104.	2.2	10.6	12.1	13.7	0.4	125.	104.	2.2
		17.7	21.6	27.3	10.4	534.	333.	7.7	14.0	17.3	31.0	2.1	110.	110.	3.2
21.0	17.7	8.0	9.2	10.4	0.4	125.	104.	1.6	8.0	9.2	10.4	0.4	125.	104.	1.6
		18.0	22.0	27.7	9.8	514.	331.	7.7	12.9	16.5	30.0	2.1	110.	110.	3.1
22.0	18.7	5.7	6.6	7.4	0.4	125.	104.	1.2	5.7	6.6	7.4	0.4	125.	104.	1.2
		16.3	21.5	30.1	9.2	495.	329.	7.4	8.6	14.3	22.2	2.1	110.	110.	2.7
23.0	19.7	3.9	4.5	5.0	0.4	125.	104.	0.8	3.9	4.5	5.0	0.4	125.	104.	0.8
		15.5	20.4	28.5	8.8	483.	326.	6.9	7.0	11.6	19.5	2.1	110.	110.	2.2
24.0	20.7	2.7	3.1	3.5	0.4	125.	104.	0.6	2.7	3.1	3.5	0.4	125.	104.	0.6
		15.0	19.7	27.6	8.4	469.	320.	6.6	5.8	9.5	17.1	2.1	110.	110.	1.8

Next, an example of VOACAP output using the PIM ionosphere:

```
IONOSPHERIC COMMUNICATIONS ANALYSIS AND PREDICTION PROGRAM
                    VOACAP    VERSION 96.0213


            1          2          3          4          5          6          7
12345678901234567890123456789012345678901234567890123456789012345678901234567890123456789012345

COMMENT     Any VOACAP default cards may be placed in the file: VOACAP.DEF
COEFFS    CCIR
TIME          1   24    1    1
MONTH      1998  617    0
SYSTEM        1. 145.  0.01  90.73.00 3.00 0.1
SUNSPOT    071.
METHOD        7    0
ANTENNA       1    1    2   30        .000[:[default]const17.voa]   .0      500.0000
ANTENNA       2    2    2   30        .000[:[default]swwhip.voa ]   .0        .0000
FREQUENCY  15.0 20.0 0.
IONOSPHERE PRISM
LABEL     Bauru                 Beverly Hills
CIRCUIT   22.32S   049.07W      34.07N    118.42W
EXECUTE
LABEL     Beverly Hills    Bauru
CIRCUIT   34.07N   118.42W      22.32S    049.07W
EXECUTE
QUIT
1     ccir Coefficients        ~METHOD  7   VOACAP 96.0213    PAGE   1

  Jun  17, 1998           SSN =  71.                Minimum Angle= 0.010 degrees
  Bauru                Beverly Hills      AZIMUTHS    N. MI.      KM
  22.32 S   49.07 W - 34.07 N  118.42 W   309.07  119.88   5205.4   9639.6

                    ELAYER/F2LAYER                        F1LAYER(E)/ESLAYER

  GMT  LMT   FOT   MUF   HPF ANGLE VIRTL   TRUE FVERT     FOT   MUF   HPF ANGLE VIRTL   TRUE FVERT

  1.0  21.7  2.0   2.3   2.6   2.1  162.   133.  0.5     2.0   2.3   2.6   2.1  162.   133.  0.5
            13.7  16.2  18.6   8.4  469.   344.  5.6     0.0   0.0   0.0   0.0    0.    0.   0.0
  2.0  22.7  1.9   2.1   2.4   3.8  198.   138.  0.5     1.9   2.1   2.4   3.8  198.   138.  0.5
            14.2  16.7  19.2   7.2  430.   317.  5.5     0.0   0.0   0.0   0.0    0.    0.   0.0
  3.0  23.7  2.2   2.6   2.9   0.3  123.   102.  0.5     2.2   2.6   2.9   0.3  123.   102.  0.5
            15.0  17.6  20.3   5.6  378.   273.  5.3     0.0   0.0   0.0   0.0    0.    0.   0.0
  4.0   0.7  2.2   2.5   2.8   0.3  122.   103.  0.4     2.2   2.5   2.8   0.3  122.   103.  0.4
            14.4  16.9  19.4   4.8  353.   260.  4.9     0.0   0.0   0.0   0.0    0.    0.   0.0
  5.0   1.7  2.2   2.5   2.8   0.2  121.   102.  0.4     2.2   2.5   2.8   0.2  121.   102.  0.4
            13.2  15.5  17.8   4.4  342.   261.  4.4     0.0   0.0   0.0   0.0    0.    0.   0.0
  6.0   2.7  2.2   2.5   2.8   0.3  122.   101.  0.4     2.2   2.5   2.8   0.3  122.   101.  0.4
            11.8  13.8  15.9   5.0  360.   279.  4.1     0.0   0.0   0.0   0.0    0.    0.   0.0
  7.0   3.7  2.2   2.5   2.8   2.4  115.   100.  0.4     2.2   2.5   2.8   2.4  115.   100.  0.4
            10.6  12.5  14.4   5.3  368.   275.  3.7     0.0   0.0   0.0   0.0    0.    0.   0.0
  8.0   4.7  2.0   2.3   2.6   2.4  167.   134.  0.5     2.0   2.3   2.6   2.4  167.   134.  0.5
             9.6  11.3  13.0   4.5  345.   252.  3.2     0.0   0.0   0.0   0.0    0.    0.   0.0
  9.0   5.7  2.1   2.4   2.7   0.3  123.   102.  0.4     2.1   2.4   2.7   0.3  123.   102.  0.4
             9.6  11.3  13.0   3.6  316.   232.  3.0     0.0   0.0   0.0   0.0    0.    0.   0.0
 10.0   6.7  2.0   2.2   2.5   0.3  123.   102.  0.4     2.0   2.2   2.5   0.3  123.   102.  0.4
            11.5  13.5  15.6   3.9  326.   241.  3.7     0.0   0.0   0.0   0.0    0.    0.   0.0
 11.0   7.7  2.2   2.5   2.8   0.5  126.   105.  0.5     2.2   2.5   2.8   0.5  126.   105.  0.5
            12.5  14.7  17.0   3.9  325.   248.  4.1     0.0   0.0   0.0   0.0    0.    0.   0.0
 12.0   8.7  2.6   3.0   3.4   0.3  121.   105.  0.5     2.6   3.0   3.4   0.3  121.   105.  0.5
            13.7  16.1  18.5   3.9  325.   246.  4.5     0.0   0.0   0.0   0.0    0.    0.   0.0
 13.0   9.7  5.4   6.2   6.9   0.4  125.   105.  1.1     5.4   6.2   6.9   0.4  125.   105.  1.1
            16.9  19.9  22.9   3.4  310.   229.  5.3     0.0   0.0   0.0   0.0    0.    0.   0.0
 14.0  10.7 12.8  14.6  16.5   2.3  113.   105.  2.7    12.8  14.6  16.5   2.3  113.   105.  2.7
            19.0  22.4  25.7   4.6  346.   224.  6.0     0.0   0.0   0.0   0.0    0.    0.   0.0
 15.0  11.7 14.0  16.0  18.1   2.4  115.   104.  2.9    14.0  16.0  18.1   2.4  115.   104.  2.9
            20.0  23.5  27.1   5.4  374.   228.  6.5     0.0   0.0   0.0   0.0    0.    0.   0.0
 16.0  12.7 15.8  18.1  20.4   0.1  117.   104.  3.2    15.8  18.1  20.4   0.1  117.   104.  3.2
            20.6  24.2  27.9   6.7  415.   238.  7.0     0.0   0.0   0.0   0.0    0.    0.   0.0
 17.0  13.7 16.5  18.9  21.3   0.1  117.   104.  3.4    16.5  18.9  21.3   0.1  117.   104.  3.4
            22.1  25.9  29.8   7.4  437.   247.  7.7     0.0   0.0   0.0   0.0    0.    0.   0.0
 18.0  14.7 17.3  19.8  22.3   0.1  117.   105.  3.5    17.3  19.8  22.3   0.1  117.   105.  3.5
            23.6  27.8  31.9   8.0  455.   255.  8.5     0.0   0.0   0.0   0.0    0.    0.   0.0
 19.0  15.7 17.0  19.4  21.9   0.1  117.   105.  3.5    17.0  19.4  21.9   0.1  117.   105.  3.5
```

```
              24.8  29.2  33.6   8.2  462.  261.   9.0    0.0   0.0   0.0   0.0    0.    0.    0.0
20.0  16.7  16.7  19.1  21.6   0.0  117.  105.   3.4   16.7  19.1  21.6   0.0  117.  105.   3.4
              25.5  30.0  34.5   8.2  462.  266.   9.4    0.0   0.0   0.0   0.0    0.    0.    0.0
21.0  17.7  15.5  17.8  20.1   0.0  116.  104.   3.2   15.5  17.8  20.1   0.0  116.  104.   3.2
              25.6  30.2  34.7   8.3  465.  270.   9.5    0.0   0.0   0.0   0.0    0.    0.    0.0
22.0  18.7   6.2   7.1   8.0   0.9  135.  119.   1.4    6.2   7.1   8.0   0.9  135.  119.   1.4
              20.0  23.5  27.1   6.8  416.  274.   7.2    0.0   0.0   0.0   0.0    0.    0.    0.0
23.0  19.7   2.7   3.1   3.4   0.7  131.  111.   0.6    2.7   3.1   3.4   0.7  131.  111.   0.6
              17.8  20.9  24.0   6.5  406.  297.   6.6    0.0   0.0   0.0   0.0    0.    0.    0.0
24.0  20.7   1.7   1.9   2.1   4.8  354.  198.   0.5    1.7   1.9   2.1   4.8  354.  198.   0.5
              15.2  17.9  20.6   7.5  439.  322.   5.9    0.0   0.0   0.0   0.0    0.    0.    0.0
```

4. REFERENCES

Anderson, D. N., A theoretical study of the ionospheric F region equatorial anomaly—Theory, *Planet. Space Sci.*, **21**, 409-419, 1973.

Anderson, D. N., The development of global, semi-empirical ionospheric specification models, in *Proceedings of the Ionospheric Effects Symposium*, J. M. Goodman, ed., pp. 353-363, 4-6 May 1993.

Brace, L. H., and R. F. Theis, Global empirical models of ionospheric electron temperature in the upper F-region and plasmasphere based on in situ measurements from the Atmospheric Explorer-C, ISIS 1, and ISIS 2 satellites, *J. Atmos. Terr. Phys.*, **43**, 1317, 1981.

Daniell, R. E., D. T. Decker, D. N. Anderson, J. R. Jasperse, J. J. Sojka, and R. W. Schunk, A Global Ionospheric Conductivity and Electron Density (ICED) Model, in *Proceedings of the Ionospheric Effects Symposium*, J. M. Goodman, ed., 1-3 May 1990.

Daniell, R. E., W. G. Whartenby, and D. N. Anderson, PRISM Validation, in *Proceedings of the Ionospheric Effects Symposium*, J. M. Goodman, ed., pp. 364-368, 4-6 May 1993.

Daniell, R. E., L. D. Brown, D. N. Anderson, M. W. Fox, P. H. Doherty, D. T. Decker, J. J. Sojka, and R. W. Schunk, Parameterized ionospheric model: A global ionospheric parameterization based on first principles models, *Radio Sci.*, **30**, 1499-1510, 1995.

Decker, D. T., C. E. Valladares, R. Sheehan, Su. Basu, D. N. Anderson, and R. A. Heelis, Modeling daytime F layer patches over Sondrestrom, *Radio Sci.*, **29**, 249-268, 1994.

Fejer, B. G., E. R. de Paula, R. A. Heelis, and W. B. Hanson, Global equatorial ionospheric vertical plasma drifts measured by the AE-E satellite, *J. Geophys. Res.*, **100**, 5769-5776, 1995.

Hardy, D. A., M. S. Gussenhoven, R. Raistrick, and W. J. McNeil, Statistical and functional representations of the pattern of auroral energy flux, number flux, and conductivity, *J. Geophys. Res.*, **92**, 12,275-12,294, 1987.

Hardy, D. A., W. McNeil, M. S. Gussenhoven, and D. Brautigam, A statistical model of auroral ion precipitation, 2, Functional representation of the average patterns, *J. Geophys. Res.*, **96**, 5539-5547, 1991.

Heppner, J. P., and N. C. Maynard, Empirical high-latitude electric field models, *J. Geophys. Res.*, **92**, 4467-4489, 1987.

Rich, F. J., and N. C. Maynard, Consequences of using simple analytical functions for the high-latitude convection electric field, *J. Geophys. Res.*, **94**, 3687-3701, 1989.

Strickland, D. J., J. S. Evans, and L. J. Paxton, Satellite remote sensing of thermospheric O/N_2 and solar EUV, 1. Theory, *J. Geophys. Res.*, *100*, 12,217-12,226, 1995.

Appendix A
PRISM Updates

Contents: PRISM changes memoranda for the period 12 August 1995 through 19 August 1996.

Memo date	PRISM version	Page
1995 August 12	1.5 to 1.5a	9
1995 September 29	1.5a to 1.6	12
1996 February 12	1.6 to 1.6a	16
1996 August 19	1.6a to 1.6b	18

M·E·M·O·R·A·N·D·U·M

DATE: *12-August-1995*

TO: *Rob Daniell*

FROM: *Lincoln Brown*

RE: *Changes to PRISM 1.5 for PRISM 1.5a*

The changes to PRISM 1.5 for PRISM 1.5a focus on a change to the Station Output File Specification requested by Hughes STX, the correction of reported problems regarding ingestion and use of DMSP and TISS data, and miscellaneous bug fixes. The changes are summarized as follows:

I.   The third header line at the beginning of the station output file has been removed and a header line added above each critical parameters data record for station output type IOUTS=0. This was requested by Hughes STX and requires a change to the Station Output File Specification.

II.   The ingestion of DMSP data has been corrected and strengthened based on problems reported by Hughes STX. PRISM can now handle up to 24 sets of each kind of DMSP data in a DMSP data file, and it can handle up to 8 DMSP data files.

III.   The ingestion of TEC data has been corrected based on problems reported by George Born's group.

IV.   Under certain conditions, several uninitialized variables in common block INDIRECT were referenced. They are now initialized in BLOCK DATA ITR4.

V.   The internal option of producing O^+ density instead of electron density on output has been removed because it was not correctly implemented.

VI.   Several subroutines that are no longer used have been removed.

The table below describes the changes that I made to PRISM 1.5 to produce PRISM 1.5a.

Module	Program Unit	Description of Changes (*Begins*)
CGM_UTIL.FOR	Subroutine BOUNDS	Removed since it is no longer used.
GETDAT.FOR	Subroutine DO_DIR	Increased the first dimension of matrix NDUMDAT from 5 to 8 to allow for 8 DMSP data files. Removed an unnecessary initialization of matrix NDUMDAT from the TEC data ingestion section. Increased the upper loop limit from 5 to 8 in the initialization of matrix NDUMDAT in the DMSP data ingestion section to allow for 8 DMSP data files.
	Subroutine DO_DMSP	Decreased PARAMETER MAXIES from 7000 to 1451 based on expected time resolutions and time windows of DMSP Ion Drift and In Situ Plasma data. Increased PARAMETER MAXJ4 from 7000 to 7211 based on the expected time resolution and time window of DMSP SSJ/4 data. Moved dummy assignment "DEN1=DEN1" from DMSP Ion Drift data ingestion section to end of routine. Changed line "GOTO 150" to "IF(NSSIES .LE. MAXIES) GOTO 150" to avoid an array-out-of-bounds error when reading a DMSP Ion Drift data set larger than the size allocated by PARAMETER MAXIES. Changed line "GOTO 214" to "IF(NSSIES .LE. MAXIES) GOTO 214" to avoid an array-out-of-bounds error when reading a DMSP In Situ Plasma data set larger than the size allocated by PARAMETER MAXIES. Changed line "goto 250" to "IF(NSSJ4 .LE. MAXJ4) GOTO 250" to avoid an array-out-of-bounds error when reading a DMSP SSJ/4 data set larger than the size allocated by PARAMETER MAXJ4. Changed line "GOTO 100" to "IF(IORB .LT. MAXORB) GOTO 100" to avoid an array-out-of-bounds error when more than MAXORB DMSP Ion Drift data sets are present in a DMSP data file. Added line "IORB=0" before line "221 CONTINUE" and line "IORB=IORB+1" after line "221 CONTINUE" to count the number of DMSP In Situ Plasma data sets in the DMSP data file. Added line "IF(IORB .LT. MAXORB) GOTO 221" before line "330 CONTINUE" to allow up to MAXORB DMSP In Situ Plasma data sets in a DMSP data file. Changed line "GOTO 300" to "IF(IORB .LT. MAXORB) GOTO 300" to avoid an array-out-of-bounds error when more than MAXORB DMSP SSJ/4 data sets are present in a DMSP data file. Changed loop upper bounds corresponding to the last dimension of common block PRECP1 arrays MLATR, MLTR, and VALTR from 2 to MAXORB because of the change in size of those arrays. Changed loop upper bounds corresponding to the last dimension of common block PRECP1 arrays LAT, MLT, and ERG from 2 to MAXORB because of the change in size of those arrays. Removed a commented-out call to subroutine GET_OVAL.
	Subroutine CONFIX	Changed PARAMETER MLATMID from 40. to 35. Changed the loop logic in the calculation of the mean midlatitude horizontal ion velocity and mean midlatitude corotation velocity to avoid an array-out-of-bounds error when no midlatitude data points are present. In the calculation of the mean midlatitude horizontal ion velocity and mean midlatitude corotation velocity, midlatitude data points are now detected by checking their calculated magnetic latitude instead of their geographic latitude. If three midlatitude data points are not available for the calculation of the mean midlatitude horizontal on velocity and mean midlatitude corotation velocity, then the data set is now ignored.
HLIM.FOR	Subroutine REGMOD	References to common block INDIRECT variable ONLYOP have been removed.
INDIRECT.INC	n/a	References to variable ONLYOP have been removed.
INIT.FOR	Subroutine INIT	Added assignments of logical flags ITR, USUE, and USUF to .TRUE. for ITY=1 when either no DISS or no high-latitude DISS data is present but high-latitude TEC data is present. This allows iteration on high-latitude TEC data in the absence of high-latitude DISS data.
	Subroutine INITPR	Removed commented-out calls to routine GET_CIRCL. Added local arrays VALTRA, MLATRA, and MLTRA. Changed the argument list in calls to routine GET_TR_KP to allow for more DMSP Ion Drift data. Added local matrices ERGA and LATA. Added local variable I. Changed the argument list in the call to routine GET_CIRCL to allow for more DMSP SSJ/4 data. Removed local variable IC since it is no longer used.
	Subroutine GET_CIRCL	Complete rewrite to allow for more DMSP SSJ/4 data.
	Subroutine GET_TR_KP	Complete rewrite to allow for more DMSP Ion Drift data.
	Subroutine CENTER	Removed since it is no longer used.
	Subroutine GET_ST_NUM	The logical flag TEC is now set to .TRUE. only if at least one TEC direct data point lies in the latitude region determined by the logical flag ITY. Previously the logical flag TEC was set to .TRUE. if any TEC direct data was present.
	Subroutine SET	Removed since it is no longer used.
	Subroutine FULL_CIRCLE	Removed since it is no longer used.
NEWFIT.INC	n/a	Changed the value of PARAMETER NMAX from 700 to 2000 to support more DMSP In Situ Plasma data. Changed the value of PARAMETER NNMAX from 2000 to 5000 to support more DMSP In Situ Plasma data.
		Continues

15

Module	Program Unit	Description of Changes (*Continued*)
OUTPUT.FOR	Subroutine WR_ST_DATA	Removed the third header line at the beginning of the station output file for station output type IOUTS=0. Added a header line above the critical parameters data record line in the station output file for station output type IOUTS=0.
PRECIP.INC	n/a	Added PARAMETER MAXORB. Changed the last dimension of common block PRECP1 arrays LAT, MLT, and ERG from 2 to MAXORB to support more DMSP SSJ/4 data. Changed the last dimension of common block PRECP1 arrays MLATR, MLTR, and VALTR from 2 to MAXORB to support more DMSP Ion Drift data.
PRISM.FOR	Block Data ITR4	Added initialization of common block INDIRECT variables HDFE, HDHE, HDF2, and HDHF2.
	Block Data PREC	Complete rewrite for more flexible initialization of arrays in common block PRECP1.
	Program PRISM	Updated the version number and version date.
Ends		

M·E·M·O·R·A·N·D·U·M

DATE: *29-September-1995*

TO: *Rob Daniell*

FROM: *Lincoln Brown*

RE: *Changes to PRISM 1.5a for PRISM 1.6*

The changes to PRISM 1.5a for PRISM 1.6 focus on the resolution of problem report PRF-PRISM19 from Bob Prochaska at Hughes STX and final enhancements for the last planned delivery of PRISM 1. The changes are summarized as follows:

I.   Problem report PRF-PRISM19 has been resolved. PRISM uses the plasma temperature to calculate a topside scale height for the midlatitude electron density, where the plasma temperature is the sum of the electron and ion temperatures from a DMSP SSIES In Situ Plasma data record. The topside scale height varies linearly with the plasma temperature. Missing electron and ion temperature data in the DMSP SSIES In Situ Plasma data record is flagged by zero values. Previously, however, if one of the temperatures was zero but the other temperature was nonzero, PRISM continued to calculate and use a plasma temperature, resulting in a topside scale height roughly half as large as it should have been. The erroneously small scale height drove the topside midlatitude electron density to fall off rapidly, resulting in very a small electron density at the top of the altitude grid. Now, PRISM ignores the temperature data in a DMSP SSIES In Situ Plasma data record and does not calculate a topside scale height for the data record if either the electron or ion temperature is zero.

II.   PRISM now checks Ionosonde (DISS) data for nonphysical values. The following tests have been added to the Ionosonde data ingestion:

A.   The observed critical frequency of the F_2 layer (f_oF_2) in the Ionosonde data record must be in the range $0 < f_oF_2 \leq 28.4$ MHz. The range maximum corresponds to a peak F_2 layer density (n_mF_2) of 10^7 cm^{-3} using the approximation $n_mF_2(\text{cm}^{-3})=1.24\times10^4 \cdot f_oF_2(\text{MHz})^2$. If the f_oF_2 parameter in the Ionosonde data record is outside this range, then the f_oF_2 parameter is ignored.

B.   The observed height of the F_2 layer (h_mF_2) in the Ionosonde data record must be in the range $200 \leq h_mF_2 \leq 1000$ km. If the h_mF_2 parameter in the Ionosonde data record is outside this range, then the h_mF_2 parameter is ignored.

C.   The observed critical frequency of the E layer (f_oE) in the Ionosonde data record must be in the range $0 < f_oE \leq 28.4$ MHz. The range maximum corresponds to a peak E layer density (n_mE) of 10^7 cm^{-3} using the approximation $n_mE(\text{cm}^{-3})=1.24\times10^4 \cdot f_oE(\text{MHz})^2$. If the f_oE parameter in the Ionosonde data record is outside this range, then the f_oE parameter is ignored.

17

D.   The observed height of the E layer (h_mE) in the Ionosonde data record must be in the range $90 \le h_mE \le 150$ km. If the h_mE parameter in the Ionosonde data record is outside this range, then the h_mE parameter is ignored.

III.   PRISM now checks TEC (IMS) data for nonphysical values. The vertical equivalent *TEC* in the TEC data record must be in the range $0 < TEC \le 250$ TEC Units (1 TEC Unit=10^{12} cm^{-2}= 10^{16} m^{-2}). If the vertical equivalent *TEC* in the TEC data record is outside this range, then the TEC data record is ignored.

IV.   PRISM now checks DMSP SSIES In Situ Plasma data for nonphysical values. The following tests have been added to the DMSP SSIES In Situ Plasma data ingestion:

A.   The in situ electron density (n_e) in the DMSP SSIES In Situ Plasma data record must be in the range $10^3 \le n_e \le 10^7$ cm^{-3}. If the n_e parameter in the DMSP SSIES In Situ Plasma data record is outside this range, then the *entire* data record is ignored.

B.   The in situ electron temperature (T_e) in the DMSP SSIES In Situ Plasma data record must be in the range $0 < T_e \le 6000$ °K. The in situ ion temperature (T_i) in the DMSP SSIES In Situ Plasma data record must be in the range $0 < T_i \le 6000$ °K. If either the electron or ion temperature in the DMSP SSIES In Situ Plasma data record is outside its range, then both temperatures are ignored.

V.   Phantom Ionosonde data has been added to PRISM. In the absence of any valid real-time Ionosonde and TEC data in 30°×30° corrected geomagnetic latitude/longitude zones between -60° and +60° corrected geomagnetic latitude, PRISM now adds phantom Ionosonde data centered in the zones to reduce the global effect of sparse real-time Ionosonde and TEC data. The phantom Ionosonde data is generated using the parameterized models in PRISM for the UT of the run, and is included in the set of real-time data that PRISM uses for its real-time adjustment of the parameterized models.

VI.   Phantom In Situ Plasma data has been added to PRISM. In the absence of any real-time SSIES In Situ Plasma data in 30°×30° corrected geomagnetic latitude/longitude zones between -60° and +60° corrected geomagnetic latitude, PRISM now adds phantom In Situ Plasma data (density only since PRISM does not contain electron and ion temperature models) centered in the zones to reduce the global effect of sparse real-time In Situ Plasma data. The phantom In Situ Plasma density data is generated using the parameterized models in PRISM for the UT of the run and DMSP altitude (840 km), and is included in the set of real-time data that PRISM uses for its real-time adjustment of the parameterized models.

VII.   Commented-out coding has been removed.

VIII.   Unused routines have been removed.

IX.   Unused variables have been removed.

The table below describes the changes that I made to PRISM 1.5a to produce PRISM 1.6.

Module	Program Unit	Description of Changes (*Begins*)
FMODEL.FOR	Subroutine FMODEL	Removed local variables TFOF2, THMF2, CFOF2, POFOF2, CFOE, and CHME since they are not used.
	Subroutine TRO_DEP	Removed local variables FOF2, HMF2, FOF2ML, and HMF2ML since they are not used.
GETDAT.FOR	Subroutine DO_DIR	Removed argument NDUMDAT(I,2) from the first call to routine DO_IONO since it is not used by that routine. Removed argument NDUM1 from the second call to routine DO_IONO since it is not used by that routine. Removed local variable NDUM1 since it is no longer used.
	Subroutine DO_IONO	Expanded the range validation of ingested E and F_2 layer Ionosonde data. Removed commented-out code for defunct BOTTOMSIDE data type. Removed PARAMETER AFPE since it is no longer used. Removed output parameter NBREC since it is no longer used.
	Subroutine DO_TEC	Expanded the range validation of ingested TEC data.
	Subroutine DO_DMSP	Expanded the range validation of ingested DMSP SSIES In Situ Plasma data. This resolves problem report PRF-PRISM19 from Bob Prochaska at Hughes STX. Removed PARAMETER TDIFMAX since it is no longer used.
	Subroutine IES_DATA	Removed since it is not used.
IO_UTIL.FOR	Subroutine CLOSFL	Removed since it is not used.
		Continues

Module	Program Unit	Description of Changes (*Continued*)
MATH_UTI.FOR	Subroutine SORT7	Removed since it is not used.
	Subroutine SWPARR	Removed since it is no longer used.
	Subroutine INDEXX	Removed since it is no longer used.
	Subroutine GETGAM	Removed since it is no longer used.
MIDLAT.FOR	Subroutine MIDLAT	Removed commented-out PRINT statements. Removed FORMAT statement 91000 since it is no longer used. Removed local variables AF and FIRST since they are no longer used.
	Subroutine PHIONO	Removed since it is not used.
	Subroutine DST1	Removed since it is no longer used.
	Subroutine PHIES	Removed since it is not used.
	Subroutine INS_TRACK	Removed since it is no longer used.
PHANTOM.FOR	n/a	New module containing routine PHANTM.
PRISM.FOR	Program PRISM	Added calls to routines INIT and PHANTM after the conversion of the nominal UT from hours to seconds. Updated the version number and version date.
READ_DBA.FOR	Subroutine READAWS	Commented out references to local variable KF000 since it is not needed.
RTA.FOR	Subroutine RTA	Removed commented-out code for bottomside fitting.
	Subroutine BOTTOM	Removed since it is not used.
STRINGS.FOR	Subroutine STRDEL	Removed since it is no longer used.
	Subroutine STRFLL	Removed since it is no longer used.
	Subroutine STRINS	Removed since it is no longer used.
	Subroutine STRNPO	Removed since it is no longer used.
	Subroutine STRRPL	Removed since it is no longer used.
	Subroutine STRSHC	Removed since it is no longer used.
	Subroutine STRSHI	Removed since it is no longer used.
	Subroutine STRTRM	Removed since it is no longer used.
	Subroutine STRUCA	Removed since it is no longer used.
	Subroutine CONCAT	Removed since it is not used.
	Subroutine DELETE	Removed since it is not used.
	Subroutine FILL	Removed since it is not used.
	Subroutine INSERT	Removed since it is not used.
	Subroutine LOCASE	Removed since it is not used.
	Subroutine LENGTH	Removed since it is not used.
	Subroutine NTHPOS	Removed since it is not used.
	Subroutine REPLAC	Removed since it is not used.
	Subroutine SHIFTC	Removed since it is not used.
	Subroutine SHIFT	Removed since it is not used.
	Subroutine TRIM	Removed since it is not used.
	Subroutine UPCASE	Removed since it is not used.
TIMELIB.FOR	Subroutine TIMMDT	Removed since it is no longer used.
	Subroutine DELTAT	Removed since it is not used.
	Subroutine GETDOY	Removed since it is not used.
	Subroutine LEAPYR	Removed since it is not used.
	Subroutine GETMDM	Removed since it is not used.
	Subroutine MODATE	Removed since it is not used.
Ends		

M·E·M·O·R·A·N·D·U·M

DATE: *12-February-1996*

TO: *Rob Daniell*

FROM: *Lincoln Brown*

RE: *Changes to PRISM 1.6 for PRISM 1.6a*

The changes to PRISM 1.6 for PRISM 1.6a focus on the replacement of the LLF parameterized model coefficients, the resolution of PRF PRISM-24, and a change to the Gridded Output Specification. The changes are summarized as follows:

I.   The LLF parameterized model coefficients have been replaced, resulting in several improvements in the low-latitude O^+ density representation in PRISM:

    A.   The solar activity dependence is now correctly represented. Previously, due to bugs in the LOWLAT theoretical model used to generate the coefficients, and misuse of one of the LOWLAT input files, no variation in the O^+ density due to solar activity level was present.

    B.   The peak of the dayside O^+ density is more in line with expected dayside densities. It is believed that the dayside electron temperature model used in LOWLAT resulted in dayside O^+ densities that were too large. The upper limit of the dayside electron temperature has been increased from 2500°K to 3000°K to maintain a smaller dayside O^+ density.

    C.   The bottomside O^+ density has been improved. Previously, spline interpolation of rapidly decreasing O^+ density on a sparse bottomside altitude grid could result in a false and substantial peak near the bottom of the LLF altitude grid (160 km). The interpolation algorithm has been modified to eliminate this problem.

II.   PRF PRISM-24 has been resolved. DMSP SSIES Ion Drift and SSJ/4 data sets are now no longer allowed to overrun allocated space in PRISM. Previously, if the maximum allowed number of data points was accepted by PRISM before the end of the dataset was reached, an array-out-of-bounds error occurred. A slight change in logic has resolved this problem. This problem was reported by Bob Prochaska at Hughes STX.

III.   The coordinate system flag IGM in the Gridded Output Specification is now consistent with the PRISM source code. Previously, the convention given in the Gridded Output Specification was opposite that used in PRISM. This problem was reported by Vince Eccles at Space Environment Corp., and its resolution was approved by Bob Prochaska at Hughes STX.

The table below describes the changes that I made to PRISM 1.6 to produce PRISM 1.6a.

Module	Program Unit	Description of Changes
GETDAT.FOR	Subroutine DO_DMSP	Changed the line "IF(NSSIES .LE. MAXIES) GOTO 150" to "IF(NSSIES .LT. MAXIES) GOTO 150" to avoid an array-out-of-bounds error when MAXIES data points in a SSIES Ion Drift data set have been accepted before the end of the data set has been reached. Changed the line "IF(NSSJ4 .LE. MAXJ4) GOTO 250" to "IF(NSSJ4 .LT. MAXJ4) GOTO 250" to avoid an array-out-of-bounds error when MAXJ4 data points in a SSJ/4 data set have been accepted before the end of the data set has been reached.
PRISM.FOR	Program PRISM	Updated the version number and version date.

M·E·M·O·R·A·N·D·U·M

DATE: *19-August-1996*

TO: *Rob Daniell*

FROM: *Lincoln Brown*

RE: *Changes to PRISM 1.6a for PRISM 1.6b*

The changes to PRISM 1.6a for PRISM 1.6b focus on improving the midlatitude real-time adjustment. The changes are summarized as follows:

I.   Several improvements have been made to the midlatitude real-time adjustment:

    A.   Real-time and phantom data that agree exactly with the parameterized models are no longer prevented from influencing the midlatitude real-time adjustment. Previously, data agreeing exactly with the parameterized models was ignored by the midlatitude real-time adjustment. This problem was reported by David Coxwell at Air Force Institute of Technology.

    B.   The actual magnetic latitude of real-time and phantom data is now used in the distance-weighting for the midlatitude real-time adjustment. Previously, the magnetic latitude of data used in the distance-weighting was normalized to the range [-90,90] degrees based on the magnetic latitude of the equatorward trough boundary. The normalization introduced error into the midlatitude correction field by artificially extending the latitudinal distance between the data and the location of interest, resulting in an elliptical rather than a circular weighting function.

    C.   The actual magnetic longitude of real-time and phantom data is now used in the distance-weighting for the midlatitude real-time adjustment. Previously, the magnetic local time of the data converted to hour angle was used in the distance-weighting. The use of the magnetic local time instead of magnetic longitude introduced as much as a 30 degree (2 hour) error in magnetic longitude in the midlatitude correction field, depending on the time difference between the data and the nominal UT.

    D.   The peak density corrections of the midlatitude real-time adjustment have been improved by using total ion densities at h_mE and h_mF_2 instead of the molecular ion density at h_mE and the O^+ density at h_mF_2. This removes the assumptions that O^+ is negligible at h_mE compared to the molecular ions and that molecular ions are negligible at h_mF_2 compared to O^+.

    E.   The density scaling correction of the midlatitude real-time adjustment has been improved by applying the E-layer and F_2-layer density scalings to both the molecular ion density profile and the O^+ density profile, resulting in a self-consistent correction. This removes the assumptions that O^+ is negligible at h_mE compared to the molecular ions and that molecular ions are negligible at h_mF_2 compared to O^+.

II.   Several minor changes have been made for compatibility with Microsoft FORTRAN. They do not impact the results.

III.   Commented-out code has been removed from several routines.

IV.   Unused FORMAT statements have been removed from several routines.

V.   Several typographical errors in comments have been corrected.

The table below describes the changes that I made to PRISM 1.6a to produce PRISM 1.6b.

Module	Program Unit	Description of Changes
MIDLAT.FOR	Subroutine MIDLAT	Removed conditionals so that data agreeing exactly with the model is not ignored in the midlatitude real-time adjustment. Magnetic local time stored in local arrays IMLT and JMLT is no longer converted to hour angle. Added local arrays IMLON and JMLON. Magnetic longitude is now stored in local arrays IMLON and JMLON. Local array JMLON is now passed to routine PER_ARR. Corrected typo in comment by changing ",HME = 8" to ",HME = 6".
	Subroutine PER_ARR	Added array JMLON to argument list. Magnetic local time stored in argument array JMLT is no longer expressed as hour angle. Magnetic latitude stored in argument array JMLAT is no longer normalized to the range [-90,90] degrees by the magnetic latitude of the equatorward trough boundary. Magnetic longitude is now stored in argument array LON instead of magnetic local time.
OUTPUT.FOR	Subroutine WRITE_DATA	Changed "1PE11.4" to ",1PE11.4" in FORMAT statement 8000 to avoid compiler error under Microsoft Fortran PowerStation. Removed commented-out code. Removed unused FORMAT statements.
	Subroutine W_ST_DATA	Removed commented-out code. Removed unused FORMAT statements, including FORMAT statement 8000, which caused a compiler error under Microsoft Fortran PowerStation.
PARAM.FOR	Subroutine PARAM	Magnetic longitude is now passed to routine RTA instead of magnetic local time by changing argument MLT to MLON in the call to routine RTA. Removed commented-out code.
PHANTOM.FOR	Subroutine PHANTM	Corrected typos in comments by changing "to added" to "to be added".
PRISM.FOR	Block Data INTRAT1	Character strings in array LABEL longer than the allocated length have been truncated. The DATA statement defining the LABEL array has been reformatted to eliminate line continuations in the middle of character strings.
	Program PRISM	Removed commented-out code. Removed unused FORMAT statements. Updated the version number and version date.
RTA.FOR	Subroutine RTA	Changed argument MLT to MLON. Variables MLAT and MLON are now passed to routine CORRECT1 instead of variables LATADJ and LTADJ. Removed local variables LATADJ and LTADJ since they are no longer used. Removed commented-out code.
	Subroutine COR_MAX	Replaced variable EE (molecular ion density at height h_mE) with argument EE+FE (total ion density at height h_mE) in the first call to routine GET_ONE_FO so that the correct ratio n_mE_{new}/n_mE_{old} (variable FRE) is returned. Removed variables NME and DNE from the first call to routine GET_ONE_FO. Replaced variable FF (O^+ density at height h_mF_2) with argument EF+FF (total ion density at height h_mF_2) in the second call to routine GET_ONE_FO so that the correct ratio $n_mF_{2,new}/n_mF_{2,old}$ (variable FRF) is returned. Removed variables NMF2 and DNF from the second call to routine GET_ONE_FO. Variables EE, EF, FE, and FF are now passed to routine DO_ADJ instead of variables DNE, DNF, and DNM. Removed local variables NME, NMF2, DNE, DNF, and DNM since they are no longer used. Removed commented-out code.
	Subroutine DO_ADJ	Complete rewrite to change algorithm and to improve coding and internal documentation. E-layer and F_2-layer density adjustments are now done on both the O^+ and molecular ion density profiles.
	Subroutine GET_ONE_FO	Removed variables NMAX and DNMAX from argument list. Removed variables NMAX and DNMAX since they are no longer used. Removed commented-out code. Removed unused FORMAT statements.
TECCALC.FOR	Subroutine LOCATE	Modified logic to eliminate .EQV. logical operator, which caused a run-time access violation error under Microsoft Fortran PowerStation.

Appendix B
Proposed Electron Temperature Model for GTIM
Robert E. Daniell, Jr.
Computational Physics, Inc.
13 August 1996

GTIM requires an electron temperature (T_e) model that may be applied independently to each flux tube. It must be realistic and mathematically well behaved. The only comprehensive empirical T_e model available are the two models of *Brace and Theis* [1978, 1981].

The Density Dependent Model

The "density dependent" model of *daytime* electron temperature, T_e, of *Brace and Theis* [1978] (hereafter B&T78) is

$$T_e(z, n_e) = c_1 + (c_2 z + c_3) \exp(c_4 z + c_5 n_e + c_6 z n_e) \tag{B.1}$$

where the six c_i are constants obtained by least squares fitting to AE-C Langmuir probe data. The values are

$$c_1 = 1051$$
$$c_2 = 17.07$$
$$c_3 = -2746$$
$$c_4 = -5.122 \times 10^{-4}$$
$$c_5 = 6.094 \times 10^{-6}$$
$$c_6 = -3.353 \times 10^{-8}$$

(Note that c_2 is given the value 17.01 in IRI-90 and *Bilitza* [1990]. I do not know which is correct.) The IRI model includes variations due to solar activity:

$$f(\overline{F_{10.7}}) = 1 + \frac{0.117 + 2.02 \times 10^{-3} \overline{F_{10.7}}}{1.0 + \exp\left[-\frac{1}{2}\left(\overline{F_{10.7}} - 102.5\right)\right]} \tag{B.2}$$

so that

$$T_e^{IRI}(z, n_e, \overline{F_{10.7}}) = T_e(z, n_e) f(\overline{F_{10.7}}) \tag{B.3}$$

It is not clear where this formula came from. No reference is given in the IRI code itself, and I have not looked up the papers in *Advances in Space Research* [*Bilitza et al.*, 1985].

We will need the altitude derivative at 400 km.

$$\frac{\partial T_e}{\partial z} = \left[c_2 + c_3 c_4 + \left(c_2 z + c_3 \right)\left(\left(c_5 + c_6 z \right)\frac{\partial n_e}{\partial z} + c_6 n_e \right) \right]\frac{T_e - c_1}{c_2 z + c_3} \qquad (B.4)$$

The AE/ISIS Model

The expression in Equation (B.1) is valid below 400 km. Above 400 km, the only model available is the spherical harmonic expansion of *Brace and Theis* [1981] (hereafter B&T81), which is based on AE data at low altitudes and ISIS data at high altitudes. This model is independent of electron density, and is provided only at four discrete altitudes: 300 km, 400 km, 1400 km, and 3000 km, which we denote by z_1, z_2, z_3, z_4, respectively. We also denote by T_i the B&T81 model temperature at z_i. The model is also independent of solar activity, but it *is* valid at all local times.

Proposed Amalgamated Brace and Theis Model

My proposal is to use the B&T78 model below 400 km, *without* the IRI-90 solar activity variation, and to use the B&T81 model at 1400 km and 3000 km with a profile that is force to match the value and derivative of the B&T78 model at 400 km. The derivative is obtained by finite difference approximation. Because the model is to be used for a flux tube, it is *not* a vertical profile. It must be continuous and smooth across the geomagnetic equator. For this reason, it will be necessary to specify T_e at the geomagnetic equator. For this purpose, I propose to use the AE/ISIS model because it is density independent.

Case 1: $z_{eq} \leq 400$ km

If the altitude of the equatorial crossing of the flux tube, $z_{eq} = L - R_\oplus$, is below 400 km, then we may use B&T78 for the entire profile.

Case 2: 400 km $< z_{eq} \leq 1400$ km

If the altitude of the equatorial crossing of the flux tube falls between 400 and 1400 km, then we have to match the high altitude profile with the B&T78 temperature and derivative at 400 km and with the B&T81 temperature at the equator.

$$\left.\frac{\partial T_e}{\partial z}\right|_{z_2} = \left.\frac{\partial T_e^{(B\&T78)}}{\partial z}\right|_{z_2}$$

$$T_e(z_2) = T_2$$

$$T_e(z_{eq}) = T_{eq} \tag{B.5}$$

A functional form meeting these requirements is

$$f(z) = T_{eq} \tanh\left[\frac{\alpha + \beta z}{(z_{eq} - z)}\right] \tag{B.6}$$

where the coefficients α and β are determined from the requirements of Equation (B.8):

$$f(z_2) = T_{eq} \tanh\left[\frac{\alpha + \beta z_2}{(z_{eq} - z_2)}\right] = T_2$$

$$\left.\frac{\partial f}{\partial z}\right|_{z_2} = \frac{\alpha + z_{eq}\beta}{(z_{eq} - z_2)^2} T_{eq} \operatorname{sech}^2\left[\frac{\alpha + \beta z_2}{(z_{eq} - z_2)}\right] = \left.\frac{\partial T_e}{\partial z}\right|_{z_2} \tag{B.7}$$

These conditions may be linearized by noting that $\operatorname{sech}^2 u = 1 - \tanh^2 u$ so that

$$\operatorname{sech}^2\left(\frac{\alpha + \beta z_2}{z_{eq} - z_2}\right) = 1 - \left(\frac{T_2}{T_{eq}}\right)^2 \tag{B.8}$$

Then the coefficient conditions become a pair of linear algebraic equations,

$$\alpha + z_2\beta = (z_{eq} - z_2)\tanh^{-1}\left(\frac{T_2}{T_{eq}}\right) \equiv \gamma_1$$

$$\alpha + z_{eq}\beta = (z_{eq} - z_2)^2 \frac{T_{eq}}{T_{eq}^2 - T_2^2}\left.\frac{\partial T_e}{\partial z}\right|_{z_2} \equiv \gamma_2 \tag{B.9}$$

which have the solution

$$\alpha = \frac{\gamma_1 z_{eq} - \gamma_2 z_2}{z_{eq} - z_2}$$

$$\beta = \frac{\gamma_2 - \gamma_1}{z_{eq} - z_2} \tag{B.10}$$

The method for obtaining the equatorial temperature is described below.

Case 3: $1400 \text{ km} < z_{eq} \le 3000 \text{ km}$

If the altitude of the equatorial crossing of the flux tube falls between 1400 and 3000 km, then we have to match the high altitude profile with the B&T78 temperature and derivative at 400 km and with the B&T81 temperatures at 1400 km and the equator.

$$\left.\frac{\partial T_e}{\partial z}\right|_{z_2} = \left.\frac{\partial T_e^{(B\&T78)}}{\partial z}\right|_{z_2}$$

$$T_e(z_2) = T_2$$

$$T_e(z_3) = T_3 \tag{B.11}$$

$$T_e(z_{eq}) = T_{eq}$$

A functional form meeting these requirements is

$$f(z) = T_{eq} \tanh\left[\frac{\alpha + \beta z + \gamma z^2}{(z_{eq} - z)}\right] \tag{B.12}$$

where the coefficients α, β, and γ are determined from the requirements of Equation (B.8):

$$f(z_2) = T_{eq} \tanh\left[\frac{\alpha + \beta z_2 + \gamma z_2^2}{(z_{eq} - z_2)}\right] = T_2$$

$$f(z_3) = T_{eq} \tanh\left[\frac{\alpha + \beta z_3 + \gamma z_3^2}{(z_{eq} - z_3)}\right] = T_3 \tag{B.13}$$

$$\left.\frac{\partial f}{\partial z}\right|_{z_2} = \frac{\alpha + z_{eq}\beta + (2z_{eq} - z_2)z_2\gamma}{(z_{eq} - z_2)^2} T_{eq} \operatorname{sech}^2\left[\frac{\alpha + \beta z_2 + \gamma z_2^2}{(z_{eq} - z_2)}\right] = \left.\frac{\partial T_e}{\partial z}\right|_{z_2}$$

These requirements may be linearized as in Case 2.

$$\alpha + z_2\beta + z_2^2\gamma = (z_{eq} - z_2)\tanh^{-1}\left(\frac{T_2}{T_{eq}}\right) \equiv \eta_1$$

$$\alpha + z_3\beta + z_3^2\gamma = (z_{eq} - z_3)\tanh^{-1}\left(\frac{T_3}{T_{eq}}\right) \equiv \eta_2 \tag{B.14}$$

$$\alpha + z_{eq}\beta + (2z_{eq} - z_2)z_2\gamma = (z_{eq} - z_2)^2 \frac{T_{eq}}{T_{eq}^2 - T_2^2}\left.\frac{\partial T_e}{\partial z}\right|_{z_2} \equiv \eta_3$$

30

The solution is obtained in the section *Solution of Equation (B.14)* below and reproduced here:

$$\alpha = \eta_1 - z_2\beta - z_2^2\gamma$$

$$\beta = \frac{\eta_2 - \eta_1}{z_3 - z_2} - (z_3 + z_2)\gamma \tag{B.15}$$

$$\gamma = \frac{1}{z_3 - z_2}\left[\frac{\eta_2 - \eta_1}{z_3 - z_2} - \frac{\eta_3 - \eta_1}{z_{eq} - z_2}\right]$$

Case 4: $z_{eq} > 3000$ km

If the altitude of the equatorial crossing of the flux tube is greater than 3000 km, then we have to match the high altitude profile with the B&T78 temperature and derivative at 400 km and with the B&T81 temperatures at 1400 km, 3000 km, and the equator.

$$\left.\frac{\partial T_e}{\partial z}\right|_{z_2} = \left.\frac{\partial T_e^{(ddm)}}{\partial z}\right|_{z_2}$$

$$T_e(z_2) = T_2$$

$$T_e(z_3) = T_3 \tag{B.16}$$

$$T_e(z_4) = T_4$$

$$T_e(z_{eq}) = T_{eq}$$

A functional form meeting these requirements is

$$f(z) = T_{eq} \tanh\left[\frac{\alpha + \beta z + \gamma z^2 + \delta z^3}{(z_{eq} - z)}\right] \tag{B.17}$$

where the coefficients α, β, γ and δ are determined from the requirements of Equation (B.11):

$$f(z_2) = T_{eq}\tanh\left[\frac{\alpha + \beta z_2 + \gamma z_2^2 + \delta z_2^3}{\left(z_{eq} - z_2\right)}\right] = T_2$$

$$f(z_3) = T_{eq}\tanh\left[\frac{\alpha + \beta z_3 + \gamma z_3^2 + \delta z_3^3}{\left(z_{eq} - z_3\right)}\right] = T_3$$

(B.18)

$$f(z_4) = T_{eq}\tanh\left[\frac{\alpha + \beta z_4 + \gamma z_4^2 + \delta z_4^3}{\left(z_{eq} - z_4\right)}\right] = T_4$$

$$\left.\frac{\partial f}{\partial z}\right|_{z_2} = \frac{\alpha + z_{eq}\beta + \left(2z_{eq} - z_2\right)z_2\delta + \left(3z_{eq} - 2z_2\right)z_2^2\delta}{\left(z_{eq} - z_2\right)^2} T_{eq}\,\mathrm{sech}^2\left[\frac{\alpha + \beta z_2 + \gamma z_2^2 + \delta z_2^3}{\left(z_{eq} - z_2\right)}\right] = \left.\frac{\partial T_e}{\partial z}\right|_{z_2}$$

These requirements may be linearized as in Cases 2 and 3.

$$\alpha + z_2\beta + z_2^2\gamma + z_2^3\delta = \left(z_{eq} - z_2\right)\tanh^{-1}\left(\frac{T_2}{T_{eq}}\right) \equiv \theta_1$$

$$\alpha + z_3\beta + z_3^2\gamma + z_3^3\delta = \left(z_{eq} - z_3\right)\tanh^{-1}\left(\frac{T_3}{T_{eq}}\right) \equiv \theta_2$$

(B.19)

$$\alpha + z_4\beta + z_4^2\gamma + z_4^3\delta = \left(z_{eq} - z_4\right)\tanh^{-1}\left(\frac{T_4}{T_{eq}}\right) \equiv \theta_3$$

$$\alpha + z_{eq}\beta + \left(2z_{eq} - z_2\right)z_2\gamma + \left(3z_{eq} - 2z_2\right)z_2^2\delta = \left(z_{eq} - z_2\right)^2\frac{T_{eq}}{T_{eq}^2 - T_2^2}\left.\frac{\partial T_e}{\partial z}\right|_{z_2} \equiv \theta_4$$

The solution is obtained in section *Solution of Equation (B.19)* below and reproduced here:

$$\alpha = \theta_1 - z_2\beta - z_2^2\gamma - z_2^3\delta$$

$$\beta = \frac{\theta_2 - \theta_1}{z_3 - z_2} - \left(z_3 + z_2\right)\gamma - \left(z_3^2 + z_3 z_2 + z_2^2\right)\delta$$

(B.20)

$$\gamma = \frac{1}{z_4 - z_3}\left(\frac{\theta_3 - \theta_1}{z_4 - z_2} - \frac{\theta_2 - \theta_1}{z_3 - z_2}\right) - \left(z_4 + z_3 + z_2\right)\delta$$

$$\delta = \frac{1}{z_4 - z_2}\left[\frac{1}{z_3 - z_2}\left(\frac{\theta_4 - \theta_1}{z_{eq} - z_2} - \frac{\theta_2 - \theta_1}{z_3 - z_2}\right) + \frac{1}{z_4 - z_3}\left(\frac{\theta_3 - \theta_1}{z_4 - z_2} - \frac{\theta_2 - \theta_1}{z_3 - z_2}\right)\right]$$

32

To obtain a vertical profile at the equator using only B&T81, since the electron density required by B&T78 is not readily available. (GTIM solves flux tubes from the top down.) We therefore require that the vertical profile meet the following requirements

$$
\begin{aligned}
T_e(z) &= T_1, \quad z \leq z_1 \\
T_e(z_2) &= T_2 \\
T_e(z_3) &= T_3 \\
T_e(z) &= T_4, \quad z \geq z_4
\end{aligned}
\tag{B.21}
$$

The following form meets these requirements

$$
f(z) = T_1 + \frac{T_4 - T_1}{2}\left\{1 + \tanh\left[\frac{\alpha + \beta z}{(z - z_1)(z_4 - z)}\right]\right\}
\tag{B.22}
$$

with the two coefficients are determined by the two conditions

$$
\begin{aligned}
f(z_2) &= T_1 + \frac{T_4 - T_1}{2}\left\{1 + \tanh\left[\frac{\alpha + \beta z_2}{(z_2 - z_1)(z_4 - z_2)}\right]\right\} = T_2 \\
f(z_3) &= T_1 + \frac{T_4 - T_1}{2}\left\{1 + \tanh\left[\frac{\alpha + \beta z_3}{(z_3 - z_1)(z_4 - z_3)}\right]\right\} = T_3
\end{aligned}
\tag{B.23}
$$

These conditions may be linearized using the inverse hyperbolic tangent:

$$
\begin{aligned}
\alpha + \beta z_2 &= \kappa_1 \equiv (z_2 - z_1)(z_4 - z_2)\tanh^{-1}\left(2\frac{T_2 - T_1}{T_4 - T_1} - 1\right) \\
\alpha + \beta z_3 &= \kappa_2 \equiv (z_3 - z_1)(z_4 - z_3)\tanh^{-1}\left(2\frac{T_3 - T_1}{T_4 - T_1} - 1\right)
\end{aligned}
\tag{B.24}
$$

These equations have the solution

$$
\begin{aligned}
\alpha &= \frac{\kappa_1 z_3 - \kappa_2 z_2}{z_3 - z_2} \\
\beta &= \frac{\kappa_1 - \kappa_2}{z_3 - z_2}
\end{aligned}
\tag{B.25}
$$

Conclusion

It is desirable that the flux tube profile be monotonically increasing above 400 km. Possible inconsistencies between B&T78 and B&T81 have to be reconciled to ensure this. In particular, when calculating the B&T81 temperature at 400 km, one must require that it be at least as large as the B&T78 temperature at 400 km before calculating the coefficients α and β for the equatorial vertical profile.

Solution of Equation (B.14)

The augmented matrix of the system (B.14) is

$$
\begin{bmatrix}
1 & z_2 & z_2^2 & \eta_1 \\
1 & z_3 & z_3^2 & \eta_2 \\
1 & z_{eq} & \left(2z_{eq}-z_2\right)z_2 & \eta_3
\end{bmatrix}
\tag{B.26}
$$

The solution is obtained using Gauss-Jordan reduction [*Hildebrand*, 1965]:

$$
\begin{bmatrix}
1 & z_2 & z_2^2 & \eta_1 \\
0 & z_3-z_2 & z_3^2-z_2^2 & \eta_2-\eta_1 \\
0 & z_{eq}-z_2 & 2\left(z_{eq}-z_2\right)z_2 & \eta_3-\eta_1
\end{bmatrix}
\tag{B.27}
$$

$$
\begin{bmatrix}
1 & z_2 & z_2^2 & \eta_1 \\
0 & 1 & z_3+z_2 & \dfrac{\eta_2-\eta_1}{z_3-z_2} \\
0 & 1 & 2z_2 & \dfrac{\eta_3-\eta_1}{z_{eq}-z_2}
\end{bmatrix}
\tag{B.28}
$$

$$
\begin{bmatrix}
1 & z_2 & z_2^2 & \eta_1 \\
0 & 1 & z_3+z_2 & \dfrac{\eta_2-\eta_1}{z_3-z_2} \\
0 & 0 & -\left(z_3-z_2\right) & \dfrac{\eta_3-\eta_1}{z_{eq}-z_2}-\dfrac{\eta_2-\eta_1}{z_3-z_2}
\end{bmatrix}
\tag{B.29}
$$

$$\begin{bmatrix} 1 & z_2 & z_2^2 & \eta_1 \\ 0 & 1 & z_3+z_2 & \dfrac{\eta_2-\eta_1}{z_3-z_2} \\ 0 & 0 & 1 & \dfrac{1}{z_3-z_2}\left[\dfrac{\eta_2-\eta_1}{z_3-z_2}-\dfrac{\eta_3-\eta_1}{z_{eq}-z_2}\right] \end{bmatrix} \qquad (B.30)$$

Back substitution yields the solutions.

$$\gamma = \frac{1}{z_3-z_2}\left[\frac{\eta_2-\eta_1}{z_3-z_2}-\frac{\eta_3-\eta_1}{z_{eq}-z_2}\right]$$

$$\beta = \frac{\eta_2-\eta_1}{z_3-z_2}-(z_3+z_2)\gamma \qquad (B.31)$$

$$\alpha = \eta_1 - z_2\beta - z_2^2\gamma$$

Solution of Equation (B.19)

The augmented matrix of the system (B.19) is

$$\begin{bmatrix} 1 & z_2 & z_2^2 & z_2^3 & \theta_1 \\ 1 & z_3 & z_3^2 & z_3^3 & \theta_2 \\ 1 & z_4 & z_4^2 & z_4^3 & \theta_3 \\ 1 & z_{eq} & (2z_{eq}-z_2)z_2 & (3z_{eq}-2z_2)z_2^2 & \theta_4 \end{bmatrix} \qquad (B.32)$$

The solution is obtained using Gauss-Jordan reduction [*Hildebrand*, 1965]:

$$\begin{bmatrix} 1 & z_2 & z_2^2 & z_2^3 & \theta_1 \\ 0 & z_3-z_2 & z_3^2-z_2^2 & z_3^3-z_2^3 & \theta_2-\theta_1 \\ 0 & z_4-z_2 & z_4^2-z_2^2 & z_4^3-z_2^3 & \theta_3-\theta_1 \\ 0 & z_{eq}-z_2 & 2(z_{eq}-z_2)z_2 & 3(z_{eq}-z_2)z_2^2 & \theta_4-\theta_1 \end{bmatrix} \qquad (B.33)$$

$$\begin{bmatrix} 1 & z_2 & z_2^2 & z_2^3 & \theta_1 \\ 0 & 1 & z_3+z_2 & z_3^2+z_3z_2+z_2^2 & \phi_{21} \\ 0 & 1 & z_4+z_2 & z_4^2+z_4z_2+z_2^2 & \phi_{31} \\ 0 & 1 & 2z_2 & 3z_2^2 & \phi_{41} \end{bmatrix} \qquad (B.34)$$

35

where $\phi_{ij} = \dfrac{\theta_i - \theta_j}{z_{i+1} - z_{j+1}}$ and $z_5 \equiv z_{eq}$.

$$
\begin{bmatrix}
1 & z_2 & z_2^2 & z_2^3 & \theta_1 \\
0 & 1 & z_3 + z_2 & z_3^2 + z_3 z_2 + z_2^2 & \phi_{21} \\
0 & 0 & z_4 - z_3 & z_4^2 + (z_4 - z_3)z_2 - z_3^2 & \phi_{31} - \phi_{21} \\
0 & 0 & -(z_3 - z_2) & -(z_3^2 + z_3 z_2 - 2z_2^2) & \phi_{41} - \phi_{21}
\end{bmatrix}
\tag{B.35}
$$

$$
\begin{bmatrix}
1 & z_2 & z_2^2 & z_2^3 & \theta_1 \\[2mm]
0 & 1 & z_3 + z_2 & z_3^2 + z_3 z_2 + z_2^2 & \phi_{21} \\[2mm]
0 & 0 & 1 & z_4 + z_3 + z_2 & \dfrac{\phi_{31} - \phi_{21}}{z_4 - z_3} \\[2mm]
0 & 0 & 1 & z_3 + 2z_2 & -\dfrac{\phi_{41} - \phi_{21}}{z_3 - z_2}
\end{bmatrix}
\tag{B.36}
$$

$$
\begin{bmatrix}
1 & z_2 & z_2^2 & z_2^3 & \theta_1 \\[2mm]
0 & 1 & z_3 + z_2 & z_3^2 + z_3 z_2 + z_2^2 & \phi_{21} \\[2mm]
0 & 0 & 1 & z_4 + z_3 + z_2 & \dfrac{\phi_{31} - \phi_{21}}{z_4 - z_3} \\[2mm]
0 & 0 & 0 & -(z_4 - z_2) & -\dfrac{\phi_{41} - \phi_{21}}{z_3 - z_2} - \dfrac{\phi_{31} - \phi_{21}}{z_4 - z_3}
\end{bmatrix}
\tag{B.37}
$$

$$
\begin{bmatrix}
1 & z_2 & z_2^2 & z_2^3 & \theta_1 \\[2mm]
0 & 1 & z_3 + z_2 & z_3^2 + z_3 z_2 + z_2^2 & \phi_{21} \\[2mm]
0 & 0 & 1 & z_4 + z_3 + z_2 & \dfrac{\phi_{31} - \phi_{21}}{z_4 - z_3} \\[2mm]
0 & 0 & 0 & 1 & \dfrac{1}{z_4 - z_2}\left[\dfrac{\phi_{41} - \phi_{21}}{z_3 - z_2} + \dfrac{\phi_{31} - \phi_{21}}{z_4 - z_3} \right]
\end{bmatrix}
\tag{B.38}
$$

Back substitution yields the solutions.

$$\alpha = \theta_1 - z_2\beta - z_2^2\gamma - z_2^3\delta$$

$$\beta = \phi_{21} - (z_3 + z_2)\gamma - (z_3^2 + z_3 z_2 + z_2^2)\delta$$

$$\gamma = \frac{\phi_{31} - \phi_{21}}{z_4 - z_3} - (z_4 + z_3 + z_2)\delta$$

$$\delta = \left[\frac{\phi_{41} - \phi_{21}}{z_3 - z_2} + \frac{\phi_{31} - \phi_{21}}{z_4 - z_3}\right]\frac{1}{z_4 - z_2}$$

(B.39)

References for Appendix B

Bilitza, D., *Solar-Terrestrial Models and Application Software*, NSSDC/WDC-A-R&S 90-19, p. 2-12, 1990.

Bilitza, D., L. H. Brace, and R. F. Theis, Modeling of ionospheric temperature profiles, *Adv. Space Res.*, *5*, 53, 1985.

Brace, L. H., and R. F. Theis, An empirical model of the interrelationship of electron temperature and density in the daytime thermosphere at solar minimum, *Geophys. Res. Lett.*, *5*, 275-278, 1978.

Brace, L. H., and R. F. Theis, Global empirical models of ionospheric electron temperature in the upper *F*-region and plasmasphere based on in situ measurements from the Atmosphere Explorer-C, ISIS 1, and ISIS 2 satellites, *J. Atmos. Terr. Phys.*, *43*, 1317, 1981.

Appendix C
Solar Activity Indices

The extreme ultraviolet (EUV) part of the electromagnetic spectrum is generally defined as wavelengths shorter than 100 nm. Let us define the quantity $Q_{EUV}^{(\lambda<\lambda_0)}$ as the energy flux of radiation with wavelengths shorter than λ_0:

$$Q_{EUV}^{(\lambda<\lambda_0)} \equiv \int_0^{\lambda} \frac{hc}{\lambda} F_{\lambda}(\lambda)d\lambda = \int_{hc/\lambda_0}^{\infty} E F_E(E) dE$$

where $F_{\lambda}(\lambda)$ is the solar photon flux per unit wavelength interval and $F_E(E)$ is the solar photon flux per unit energy interval. Since the ionization thresholds for O and H are both near 91 nm, and the ionization thresholds for O_2 and N_2 are near 103 nm and 80 nm, respectively, the quantity $Q_{EUV} \equiv Q_{EUV}^{(\lambda<100\ nm)}$ is a natural choice for a solar activity index that tracks the impact of solar variability on the ionosphere.

The most widely used reference solar EUV spectrum is that of *Hinteregger et al.* [1981], known as SC#21REF, derived from both rocket and satellite data during solar cycle 21. Plots of $Q_{EUV}^{(\lambda<\lambda_0)}$ calculated from this spectrum are shown in Figure C.1 for two levels of solar activity as indexed by $F_{10.7}$. These plots illustrate that the overall shape of the spectrum does not vary dramatically with solar activity: a doubling of $F_{10.7}$ results in a doubling of $Q_{EUV}^{(\lambda<\lambda_0)}$ mostly independent of the choice of cutoff wavelength λ_0.

Strickland et al. [1995] have proposed a method for remote sensing of the solar extreme ultraviolet (EUV) flux by monitoring thermospheric dayglow emissions from space. The SSUSI instrument, which will be aboard a number of DMSP satellites to be launched near the end of this decade and into the next century, will monitor the dayglow and an algorithm has been developed to derive the EUV flux from those measurements. Specifically, the quantity to be reported is $Q_{EUV}^{(\lambda<45)}$, the integrated energy flux at wavelengths shortward of 45 nm in units of erg cm^{-2} s^{-1}, since this is the wavelength range to which the dayglow emissions are most sensitive.

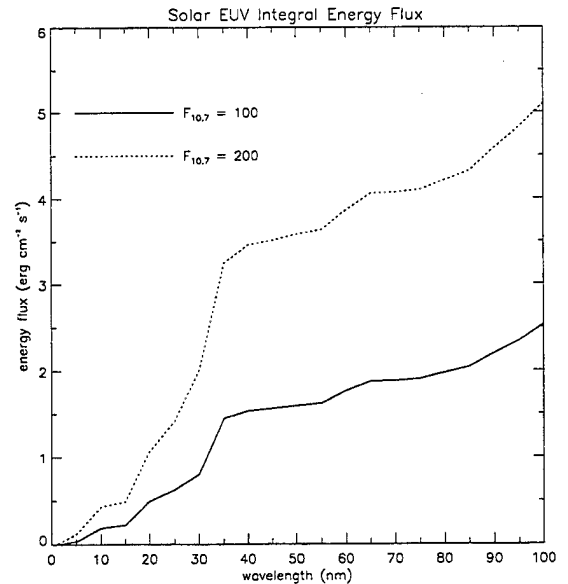For the reasons described above, we would prefer to have $Q_{EUV}^{(\lambda<100)}$, the energy flux

Figure C.1. The integral solar EUV flux $Q_{EUV}^{(\lambda<\lambda_0)}$, as a function of λ_0, for two levels of solar activity (indexed by $F_{10.7}$) as derived from the Hinteregger reference spectrum SC#21REF.

shortward of 100 nm (that is, the total EUV energy flux). However, it should be possible to convert between the $Q_{EUV}^{(\lambda<100)}$ and $Q_{EUV}^{(\lambda<45)}$ with greater confidence than converting between $F_{10.7}$ and $Q_{EUV}^{(\lambda<100)}$. The conversion is simply

$$Q_{EUV}^{(\lambda<100)} \approx 1.5\, Q_{EUV}^{(\lambda<45)}$$

Until SSUSI or some alternative instrument is actually returning $Q_{EUV}^{(\lambda<45)}$ in near real time, however, we will have to continue to rely on $F_{10.7}$ as an indicator of solar activity. In that case, we convert from $F_{10.7}$ to $Q_{EUV}^{(\lambda<100)}$ using the formula.

$$Q_{EUV}^{(\lambda<100)} \approx 0.026\, F_{10.7} - 0.1$$

with $F_{10.7}$ in solar flux units (10^{-22} W m^{-2} Hz^{-1}) and $Q_{EUV}^{(\lambda<100)}$ in erg cm^{-2} s^{-1}.

References for Appendix C.

Hinteregger, H. E., K. Fukui, and B. R. Gilson, Observational, reference and model data on solar EUV, from measurements on AE-E, *Geophys. Res. Lett.*, *8*, 1147-1150, 1981.

Strickland, D. J., J. S. Evans, and L. J. Paxton, Satellite remote sensing of thermospheric O/N$_2$ and solar EUV, 1. Theory, *J. Geophys. Res.*, *100*, 12,217-12,226, 1995